Postprint: Simulation Study on Key Device Parameters for High-Precision Fabry-Perot Cavity Resonant Frequency Drift Tracking System

Authors: Liu Tongjun, Ye Huiqi, Tang Liang, Xiao Dong

Date: 2025-10-11T14:37:56+00:00

Abstract

In recent years, broadband Fabry-Perot (FP) cavities have been widely employed in high-precision astronomical spectral calibration; achieving long-term spectral calibration precision better than 1 m/s using FP cavities requires stability better than 10^-9 (i.e.

Instrument: Fabry-Perot cavity|Instrument: Rubidium absorption cell|Instrument: External cavity semiconductor laser|Technique: Radial velocity

Classification:

Astronomy

>>

Astronomy

Journal: Acta Astronomica Sinica

Submission Status: Published in journal

Citation:

ChinaXiv:202510.00052

DOI:10.15940/j.cnki.0001-5245.2025.05.010 CSTR:32003.36.ChinaXiv.202510.00052

Full Text

Preamble

Vol. 66 No. 5

September 2025

ACTA ASTRONOMICA SINICA Vol. 66 No. 5 Sept., 2025 doi: 10.15940/j.cnki.0001-5245.2025.05.010

Simulation Study on Key Device Parameters of High-precision Fabry-Perot Cavity Resonant Frequency Drift Tracking System

LIU Tong-jun[1,2,3] YE Hui-qi[1,2] TANG Liang[1,2] XIAO Dong[1,2]†

(1 Nanjing Institute of Astronomical Optics & Technology, Chinese Academy of Sciences, Nanjing 210042)

(2 Key Laboratory of Astronomical Optics & Technology, Chinese Academy of Sciences, Nanjing 210042)

(3 University of Chinese Academy of Sciences, Beijing 100049)

Abstract

Broadband Fabry-Perot (FP) cavities have been widely employed in high-precision astronomical spectral calibration in recent years. Achieving spectral calibration accuracy better than 1 m/s requires FP cavity stability better than 10 (<MHz). However, coating aging, phase transitions of spacer materials, and long-term environmental variations all contribute to slow drift of FP spectral lines, compromising the long-term repeatability of wavelength calibration. To improve long-term calibration accuracy, we designed a high-precision laser scanning tracking system that uses a rubidium absorption cell as an absolute frequency reference. The system utilizes a small free spectral range (FSR) auxiliary FP cavity combined with rubidium absorption lines to precisely calibrate the laser scanning frequency. To determine the optimal auxiliary FP cavity parameters, we simulated the frequency calibration performance of

FP cavities made from two different materials with various FSR values under different detection conditions (temperature variations and noise levels). The results demonstrate that, without considering environmental and detection factors, an FSR of 70 MHz or below can achieve frequency calibration with MHz-level accuracy. Meanwhile, smaller FSR values exhibit greater sensitivity to temperature changes and detection noise. Considering both the simulation results and fabrication challenges, the optimal scanning frequency calibration FP cavity is a hollow-core fiber FP cavity with an FSR of 30–70 MHz.

Key words instrumentation: Fabry-Perot cavity, instrumentation: rubidium absorption cell, instrumentation: external cavity diode lasers, techniques: radial velocities

CLC number: P111 **Document code:** A

1 Introduction

The Fabry-Perot (FP) cavity is an optical resonator composed of two parallel reflective surfaces that selectively transmits specific wavelengths, making it widely applicable in frequency filtering [1–2], sensing [3–4], displacement measurement [5], and wavelength calibration [6–8]. The resonant frequency of an FP cavity depends on the cavity' s refractive index and length, and environmental temperature and pressure variations affect these physical parameters, causing resonant frequency drift. While sensing applications leverage this drift to measure target parameters, wavelength calibration suffers from degraded accuracy due to such drift. The radial velocity method detects exoplanets by measuring the Doppler shift in stellar spectra caused by planetary orbital motion, requiring high-precision wavelength calibration—for instance, detecting Earth-like planets around Sun-like stars demands radial velocity measurement precision of 9 cm/s maintained over a year. High-precision wavelength calibration methods [9] primarily include astronomical frequency combs, continuous light sources paired with FP cavities, and hollow cathode lamps. Using a continuous light source with an FP cavity generates a series of densely distributed transmission peaks that are approximately equally spaced in the frequency domain. This approach offers advantages of system simplicity and higher short-term calibration precision than Th-Ar lamps, but FP cavities are susceptible to environmental influences that cause resonant frequency drift. Even well temperature- and pressure-controlled air-gap FP cavities exhibit daily drift exceeding 10 cm/s (corresponding to hundreds of kHz) [10], leading to degraded long-term calibration accuracy. High-precision (MHz-level) tracking of FP cavity resonant frequency drift is therefore essential to improve long-term calibration performance, making the precise tracking of FP cavity resonant frequency drift a critical challenge. Scanning the FP cavity with an external cavity laser represents a relatively direct approach to resonant frequency tracking.

External cavity tunable lasers utilize a diffraction grating and laser cavity mirror to form an external resonator, with piezoelectric ceramics adjusting the

grating angle to tune the output wavelength. These lasers offer high output power, narrow linewidth, and wide tuning range, making high-resolution FP cavity transmission spectra obtainable through frequency scanning. However, external cavity lasers suffer from nonlinear scanning frequency variation with piezoelectric ceramic drive voltage [11], primarily due to piezoelectric hysteresis and creep. Directly assuming a linear relationship between laser scanning frequency and scanning time (drive voltage and scanning time are generally linearly related) introduces errors, necessitating auxiliary methods to obtain high-precision frequency-time relationships. Current approaches primarily involve using additional frequency references to calibrate the scanning frequency at each moment. These include scanning Mach-Zehnder interferometers [12], FP cavities [13], fiber ring cavities [14] with small FSR values ranging from several MHz to hundreds of MHz, using interference peaks to calibrate frequency-time relationships, or beating with high-precision frequency combs [15] to calibrate scanning frequency using individual comb teeth. Compared with optical frequency comb systems, resonant cavities like FP or ring cavities offer lower system complexity. Although their frequency accuracy is lower than comb systems, they can achieve 10 or even higher frequency precision when combined with elemental absorption cells. Compared with Mach-Zehnder interferometers, FP cavity resonant peaks are generated through multiple-beam interference, providing better peak contrast and making them more suitable as frequency reference standards. The peak spacing in the frequency domain is primarily determined by the FSR, with smaller FSR corresponding to larger optical path length. Overly long cavities impose higher demands on fabrication and environmental stability, making the selection of appropriate FP cavity parameters crucial for achieving high-precision stable external cavity laser frequency calibration.

This paper designs a high-precision frequency scanning system based on an external cavity laser, rubidium absorption cell, and scanning frequency calibration FP cavity to track resonant frequency drift in astronomical wavelength calibration FP cavities with MHz-level accuracy. Through experiments and simulations, we optimized the parameters of the key system component—the scanning frequency calibration FP cavity. First, we determined the relationship between external cavity laser frequency and scanning time through measurements and literature review, then simulated frequency calibration performance using scanning frequency calibration FP cavities with different FSR values and finesse. Building upon this, we further considered temperature variations and detection noise, simulating frequency calibration performance for two different FP cavity materials under various temperature changes and noise levels. Combining these results with fabrication difficulty considerations, we identified the material and parameters for the scanning frequency calibration FP cavity that meet the design objectives.

2 Theoretical Background and Simulation Methods

2.1 Fundamental Principles of Fabry-Perot Cavities

The schematic diagram of an FP cavity is shown in

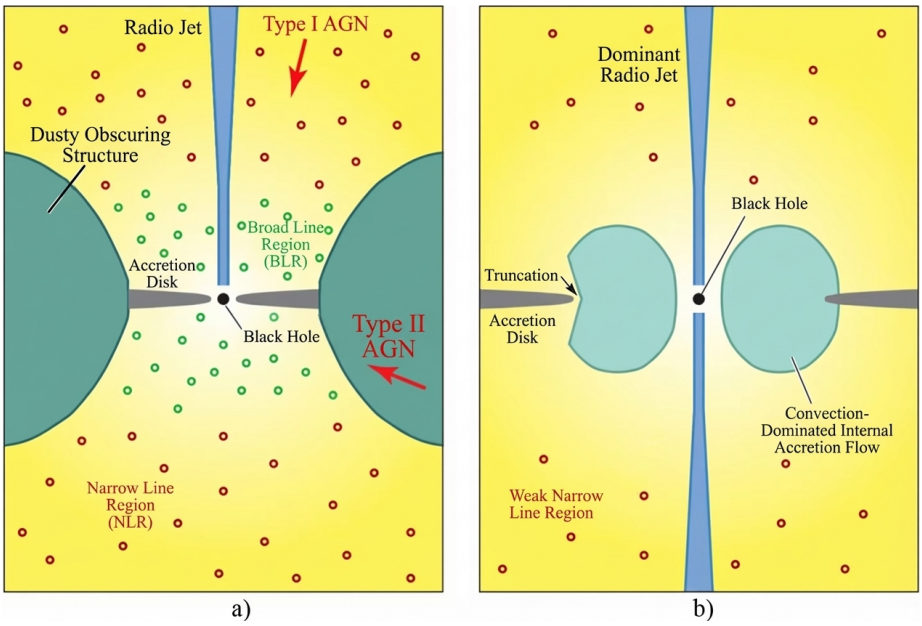

Figure 1: Figure 1

. The cavity consists of two parallel mirrors with reflectivity R at both ends. Light entering from one end undergoes multiple reflections between the mirrors, with a portion transmitted through the right mirror during each reflection. The total transmitted light represents the coherent superposition of each transmitted component. Assuming mirror reflectivity R, transmittance T, initial electric field E , wavelength , incident angle , cavity length d, and cavity refractive index n, the transmitted electric field after multiple coherent superpositions can be expressed as:

$$E_t = E_0(1-R)\sum_{m=1}^{\infty} R^m \exp\left(i\frac{4\pi}{\lambda}mdn\cos\theta\right) \tag{1}$$

where m represents the number of times light passes through the second mirror. After obtaining the electric field distribution of transmitted light through Eq. (1), the total transmitted intensity I can be calculated from the complex electric field magnitude:

$$I_t = |E_t|^2 \tag{2}$$

Using Eq. (2), we calculate the transmitted intensity for given parameters. By varying the wavelength parameter in Eq. (1), we can compute the intensity distribution across a wavelength or frequency range.

2.2 Simulation of External Cavity Laser Scanning FP Cavity and Frequency Fitting

External cavity lasers achieve frequency scanning resolution of 50 kHz or higher in mode-hop-free operation, but the frequency-time relationship is nonlinear due to piezoelectric ceramic characteristics. Assuming the laser frequency v is a function of time t, $v = f(t)$, and combining this with the known intensity distribution of the FP cavity in the frequency domain, we map this frequency-domain intensity distribution onto the time domain:

$$I_t = g(v) = g(f(t)) \tag{4}$$

This yields the external cavity laser scanning results. For cases where the frequency-time function cannot be expressed analytically, numerical one-to-one mapping can be employed by first determining the frequency value corresponding to each scanning sampling point, then obtaining the transmitted intensity at that sampling moment based on the frequency value.

After obtaining simulated scanning results, we must evaluate the frequency calibration performance by fitting the frequency-time relationship from these results and assessing the fitting accuracy through comparison with set values. Frequency calibration relies on the assumption that the absolute frequencies at rubidium absorption peaks and the FSR of the scanning frequency calibration FP cavity remain essentially constant across the scanning range. As illustrated in the flowchart [FIGURE:2], we first locate rubidium absorption peaks and assign frequency values based on their characteristics, establishing a one-to-one correspondence between these scanning points N , N , ⋯, N and absolute frequencies f , f , ⋯, f . We then identify the two nearest FP cavity transmission peaks corresponding to scanning points N and N , perform local linear fitting using the rubidium peak scanning points and their corresponding frequencies to assign frequencies f and f to these selected FP cavity peaks, and calculate the FP cavity FSR based on the mode number difference and frequency interval between these two peaks. Assuming uniform FSR across the scanning band, we determine the frequency for each FP cavity peak. Finally, we employ univariate spline fitting to obtain the relationship between FP cavity peaks and corresponding scanning points. Comparing the fitted results with set values allows evaluation of the fitting performance.

2.3 Modeling Temperature Variation and Detection Noise Effects on Frequency Fitting

Temperature variations affect the refractive index and cavity length of FP cavities, causing transmission peak frequency drift. External cavity lasers acquire FP cavity transmission spectra through frequency scanning, meaning different frequencies are not obtained simultaneously. If temperature changes during the detection period, the measurement results will correspondingly vary, undermining the FSR uniformity assumption and affecting measurement precision. To simulate temperature effects, we first determine the temperature range and cavity material, then obtain the corresponding cavity length and refractive index at each temperature based on the material' s thermal expansion coefficient and thermo-optic coefficient. Using the method described in Section 2.2, we compute scanning results at different temperatures to form a data matrix, then select corresponding data from this matrix according to the temperature-time relationship to obtain scanning results with temperature variation. The schematic for selecting data from the matrix is shown in [FIGURE:3].

In addition to temperature effects, noise also impacts fitting precision. Throughout the detection system, noise originates from various sources including photon noise from the light source, detector dark current, and thermal noise. Following the approach in reference [16], we simplify the noise model to two types: Poisson-distributed noise related to signal intensity and Gaussian-distributed noise independent of signal intensity. Poisson noise represents photon noise, while Gaussian noise represents various photodetector noises. Poisson noise magnitude can be estimated from actual light source parameters. Due to the characteristic that relative fluctuations decrease with increasing signal intensity, Poisson noise fluctuations are less than 1% relative to the original signal when the detector receives 0.1 mW at maximum FP cavity transmittance—significantly smaller than the added Gaussian noise. Consequently, Gaussian noise independent of intensity dominates. After adding noise, the magnitude is evaluated using the signal-to-noise ratio (peak FP cavity transmission relative to noise in decibels).

3 System Design and Parameter Selection for Scanning Frequency Calibration FP Cavity

3.1 System Design Description

The FP cavity resonant frequency drift tracking system is illustrated in [FIGURE:4]. The external cavity tunable laser serves as the frequency-swept light source with a mode-hop-free scanning range of 40 GHz. The laser output splits into three paths passing through a rubidium absorption cell, a scanning frequency calibration fiber FP cavity, and a wavelength calibration FP cavity to obtain rubidium absorption spectra, fiber FP cavity transmission spectra, and target FP cavity transmission spectra, respectively. The wavelength calibration FP cavity will be used for synchronous calibration of astronomical spectro-

graphs. In addition to the swept laser, the input light source includes a white light source for calibration. The swept laser is separated by a filter after transmitting through the wavelength calibration FP cavity for detection, while the remaining transmitted light enters the spectrograph for wavelength calibration. The scanning frequency calibration fiber FP cavity employs an anti-resonant hollow core fiber structure. The fabrication method follows reference [17], utilizing graded-index fiber for high-efficiency light transmission with single-mode fiber, with reflective coatings applied to the graded-index fibers at both ends of the hollow core fiber to form the resonant cavity. This fabrication method enables FP cavities with high finesse (>100). The absolute laser frequency at each scanning moment can be determined using the first two spectral lines as described in Section 2.2. With the laser frequency at each scanning moment established, we can obtain the central frequency, full width at half maximum, and other information for one or several modes of the wavelength calibration FP cavity during that scan. Repeated scans over time enable tracking of the drift in central frequencies of these transmission modes.

The system' s target accuracy requires achieving frequency precision at the MHz level within the scanning range during a single scan. To satisfy this objective, an appropriate fiber FP cavity must be selected. Section 3.2 determines the magnitude and manifestation of external cavity laser scanning nonlinearity through experimental measurements and literature review. Section 3.3 simulates frequency fitting performance using FP cavities with different FSR values and finesse in conjunction with rubidium absorption cells. Section 3.4 further incorporates temperature variations and noise levels during detection into the simulation, ultimately selecting the scanning frequency calibration FP cavity parameters based on the target accuracy and simulation results.

3.2 Determination of Scanning Nonlinearity

To determine the scanning frequency calibration FP cavity parameters, we first obtained the relationship between external cavity laser frequency and scanning time. Using a Toptica external cavity laser DL pro, we scanned a 1.5 GHz FSR FP cavity (Thorlabs SA200-5B) and a Toptica Cosy rubidium absorption module, obtaining the scanning results shown in FIGURE:5. Based on rubidium spectral characteristics, we selected prominent peaks from the first two peak groups in the rubidium absorption spectrum as characteristic points and assigned frequencies corresponding to Rb 5S F=2 → Rb 5P CO CO F=3 and Rb 5S F=3 → Rb 5P CO CO F=4 transitions (CO denotes cross-absorption peaks to two energy levels).

We performed linear fitting on the relationship between piezoelectric ceramic drive voltage and external cavity laser frequency using these peak voltage-frequency relationships, with results shown in FIGURE:5. The straight line represents the linear fitting result, while the asterisk markers indicate selected rubidium peak positions. Using the method described in Section 2.2, we assigned frequencies to FP cavity peaks based on rubidium peak frequencies and

the assumption of equal frequency spacing between FP cavity peaks, represented as circles in FIGURE:5. These frequency values gradually deviate from the linear fitting result, allowing estimation of large-scale scanning nonlinearity magnitude and form through the distribution of these peak points. FIGURE:5 displays the difference between FP cavity peak frequencies and the linear fitting frequencies, revealing that FP cavity peaks deviate from the linear fitting by up to 500 MHz across a 10 GHz scanning range (approximately corresponding to 20 V piezoelectric ceramic drive voltage variation), with the difference distribution approximating a quadratic function. We therefore propose using a quadratic function to simulate large-scale scanning nonlinearity.

According to reference [12], external cavity lasers also exhibit smaller-scale local scanning nonlinearity. This reference used both a 1.5 GHz FSR FP cavity and a 5 MHz FSR Mach-Zehnder interferometer to characterize external cavity laser scanning nonlinearity, with the Mach-Zehnder interferometer results reflecting local nonlinearity characteristics. No clear theoretical model exists for this local nonlinearity; we selected superposition of trigonometric functions to simulate these features based on observed characteristics (local nonlinearity fluctuations ranging from tens to hundreds of MHz without clear periodicity). This approach approximates both the amplitude variation and general pattern of actual measurements. By adjusting parameters, we obtained results closely matching the local nonlinearity magnitude and form reported in the literature, as shown in [FIGURE:6].

The frequency range in [FIGURE:6] is 1.5 GHz. The dashed line represents the sampling point-frequency relationship generated from the 1.5 GHz FSR FP cavity results, while the solid line shows the result after adding local scanning nonlinearity simulated through a series of trigonometric functions. The result with added local nonlinearity exhibits tens-of-MHz-scale fluctuations compared with the original, closely matching reported experimental results and validating our simulation parameters. In summary, we modeled external cavity laser frequency-time variation through experimentally measured large-scale scanning nonlinearity distribution combined with literature-based simulation of local nonlinearity (which cannot be measured under current experimental conditions). The large-scale nonlinearity was measured using a 1.5 GHz FSR FP cavity, while local nonlinearity within smaller ranges was simulated based on literature measurements.

3.3 Simulation Results for Different Scanning Frequency Calibration FP Cavity Parameters

Building upon the scanning nonlinearity distribution obtained in Section 3.2, we generated simulated transmission spectra for external cavity lasers scanning FP cavities with FSR values of 10, 30, 70, 150, 300, 750, and 1500 MHz using the method described in Section 2.2. The simulation used 25,000 sampling points across a 10 GHz scanning range, corresponding to a frequency scanning resolution of 400 kHz, consistent with external cavity laser capabilities. The

scanning frequency calibration FP cavity finesse was set to approximately 20. Simulated scanning results for 1500 MHz and 150 MHz FSR are shown in FIGURE:7. The non-uniform intervals between peaks in the 150 MHz FSR FP cavity transmission spectrum result from the nonlinear frequency variation of the external cavity laser with sampling time. Using these simulated scanning results combined with rubidium absorption lines and the method from flowchart [FIGURE:2], we can obtain the laser frequency-time (sampling point) relationship.

The frequency fitting error magnitude using different FSR FP cavities combined with rubidium absorption spectra is shown in FIGURE:7. For large FSR values such as 1500 MHz and 750 MHz, the system cannot resolve local scanning nonlinearity, with differences between set values reaching approximately 40 MHz—insufficient to meet the MHz-level absolute frequency accuracy requirement. As FSR decreases, the error diminishes, achieving satisfactory results at 70 MHz and below, meeting the target accuracy. This indicates that, under current scanning nonlinearity settings, achieving target frequency precision requires the FP cavity FSR to reach 70 MHz or below. This result corresponds to the magnitude and fluctuation characteristics of local nonlinearity shown in FIGURE:7. According to the Nyquist sampling theorem, when sampling points exceed twice the highest frequency of the original signal, the original signal can be reconstructed from discrete samples. Since the local nonlinearity approximate period is around hundreds of MHz, only FSR values of 70 MHz or below can resolve local nonlinearity. This implies that if the local nonlinearity pattern changes, the appropriate scanning frequency calibration FP cavity FSR will also change.

Beyond FSR, finesse may also affect final fitting precision. Assuming identical material and length for FP cavities with the same FSR, finesse is primarily determined by the reflectivity R of the cavity mirrors. We generated results for finesse values ranging from 4 to 60 by varying R. Simulated results and fitting errors for 10 MHz FSR FP cavities with different finesse are shown in FIGURE:7 and (d). For finesse between 4 and 20, fitting errors remain essentially consistent. At finesse above 60, the single-peak full width at half maximum becomes too narrow relative to the limited laser scanning resolution, causing fitting errors that affect precision. Therefore, scanning frequency calibration FP cavity finesse must be matched with external cavity laser scanning performance, and excessively high finesse should be avoided when FSR is small.

3.4 Effects of Temperature Fluctuations and Noise

Based on simulation conclusions from Section 3.3, FP cavities with FSR below 70 MHz can achieve MHz-level frequency accuracy under current settings without considering other factors. However, in practice, smaller FSR corresponds to longer cavity length, making the system more sensitive to environmental changes, necessitating consideration of temperature variations during scanning. External cavity laser scanning typically completes within less than one second,

so temperature variation during a single scan is minimal. Assuming temperature fluctuations of 3 mK, 10 mK, and 40 mK relative to a baseline of 293 K (20°C) during one scan, the temperature at different sampling points is shown in [FIGURE:8], with minimum temperature variation set to 10 K.

Fiber cavities facilitate achieving long cavity lengths, with common implementations including conventional silica single-mode fiber FP cavities and hollow core fiber (HCF) FP cavities. We simulated both types, modeling the hollow fiber as an anti-resonant hollow core fiber. For such fibers, the thermo-optic coefficient in the fiber core is primarily determined by the gas composition within the fiber [18], so we used silica parameters for thermal expansion coefficient calculation and air parameters for thermo-optic coefficient. Single-mode fiber parameters were based on silica. Specific values for thermal expansion coefficient, thermo-optic coefficient, and other parameters for air and silica at 293 K (20°C) are listed in .

Using these parameters and the method from Section 2.3, we generated simulated scanning results for different FSR values (same parameters as Section 3.3) and two material types under three temperature variation scenarios, forming data matrices from which we selected data according to the temperature-time relationship in [FIGURE:8]. Results for 300 MHz FSR hollow core fiber and single-mode fiber FP cavities under 40 mK temperature variation are shown as examples in [FIGURE:9]. Due to temperature variations, the central frequencies of FP cavity transmission peaks drift during laser frequency scanning, altering the intervals between obtained transmission peaks while leaving peak full width at half maximum relatively unchanged. Single-mode fiber exhibits an order-of-magnitude larger drift than hollow core fiber due to greater material temperature sensitivity, consistent with existing experimental measurements [17]. This drift undermines the assumption of equal frequency spacing between peaks, affecting the precision of frequency-time relationship fitting.

For better comparison, we present fitting results with and without temperature fluctuations, showing only FSR values of 70 MHz and below. Fitting errors for 10 MHz, 30 MHz, and 70 MHz FSR fiber FP cavities under different temperature fluctuations are shown in [FIGURE:10]. The 拐点 (inflection points) at both ends of the fitting results in [FIGURE:10] are inherent characteristics of spline fitting, affecting only a few sampling points at the edges and having minimal impact on tracking actual FP cavity transmission peaks with certain widths. We therefore focus on non-edge regions. For a given material and FSR (within each subplot), larger temperature variations during a single scan produce greater fitting errors. Comparing across subplots FIGURE:10, (c), and (e) for the same material but different FSR values reveals that smaller FSR (longer cavity length) experiences greater effects under identical temperature influence. Comparing horizontally across subplots for the same FSR but different materials shows that anti-resonant hollow core fiber cavities experience smaller effects under identical temperature variations. For a 70 MHz FSR hollow core fiber FP cavity, temperature variations must be near or below 10 mK during a sin-

gle scan to ensure temperature-induced fitting errors approach or remain below MHz level, whereas single-mode fiber cavities have more stringent temperature requirements—even 3 mK variation fails to meet requirements for 70 MHz FSR.

After simulating temperature effects, we also modeled detection noise impact. Noise composition and addition methods follow Section 2.3. We evaluated noise magnitude using signal-to-noise ratio (peak FP cavity transmission relative to noise in decibels) ranging from 40 dB to below 10 dB. Fitting differences between results and set values for 10 MHz, 30 MHz, and 70 MHz FSR FP cavities under various detection noise levels are shown in [FIGURE:11]. Except for the 10 MHz FSR FP cavity results, other FSR values show significant fitting errors only when signal-to-noise ratio falls below 10 dB (specifically 8 dB). The 10 MHz FSR case is more sensitive to noise, showing obvious fitting errors when signal-to-noise ratio falls below 20 dB. We further increased sampling points for 10 MHz FSR FP cavity simulation to 100,000 (four times the original), with fitting results shown in [FIGURE:12]. Comparison between FIGURE:11 and (b) reveals that more sampling points enable tolerance of greater noise. This indicates that smaller FSR FP cavities are more noise-sensitive primarily because fewer sampling points per peak affect single-peak recognition and fitting. With fewer sampling points per peak, noise tolerance decreases. In practice, sampling points are limited by laser scanning resolution, computational capacity, and other factors, so ensuring adequate signal-to-noise ratio is essential for achieving target precision when FSR is small and sampling points are limited. Considering both temperature and noise effects, smaller FSR imposes higher demands on environment and detection. Combined with increased fabrication difficulty for longer cavities, we conclude that anti-resonant hollow core fiber FP cavities with FSR of 30–70 MHz are most suitable as scanning frequency calibration tools.

4 Conclusion

To improve the long-term precision of FP cavity wavelength calibration, this paper designed a high-precision FP cavity resonant frequency drift tracking system based on an external cavity laser. The system uses a rubidium absorption cell combined with a hollow core fiber FP cavity to calibrate the external cavity laser frequency-time relationship, enabling high-precision tracking of wavelength calibration FP cavity resonant frequency drift. Meter-per-second-level radial velocity measurement precision requires MHz-level frequency accuracy. To achieve this accuracy target, we conducted extensive simulations to determine parameters for the key system component—the scanning frequency calibration FP cavity. Without considering temperature and detection noise effects, FP cavities with FSR 70 MHz and finesse that does not affect single-peak fitting can achieve MHz-level frequency calibration in conjunction with rubidium absorption cells, meeting system design objectives. When further considering temperature fluctuations and detection noise, anti-resonant hollow core fiber cavities are more suitable as scanning frequency calibration FP cavities due to their relatively

small thermo-optic coefficients. Regarding FSR selection, smaller FSR exhibits greater temperature sensitivity and imposes higher environmental control requirements, so the final FSR should not be excessively small. Concerning noise, since external cavity laser frequency scanning resolution has limits, smaller FSR produces denser peaks and fewer sampling points per peak, making fitting more susceptible to noise. Considering temperature and noise factors along with fabrication difficulty, achieving MHz-level frequency accuracy requires scanning frequency calibration FP cavities with FSR of 30–70 MHz and finesse of 10–30 using anti-resonant hollow core fiber, under adequate temperature control. This high-precision scanning frequency system can be applied to track resonant frequency drift in high-precision wavelength calibration FP cavities and provides a foundation for studying long-term FP cavity resonant frequency drift. Additionally, due to its high frequency precision characteristics, the system can be applied to determine transmission frequencies of solar filter FP cavities, high-precision spectral measurements, high-precision scanning frequency interferometric ranging, and other applications requiring high precision in absolute or relative frequency changes.

Acknowledgments

We thank the reviewers for their valuable suggestions, which significantly improved the quality of this paper.

References

1. Milne J S, Dell J M, Keating A J, et al. *JMemS*, 2009, 18: 905
2. Steinmetz T, Wilken T, Araujo-Hauck C, et al. *ApPhB*, 2009, 96: 251
3. Islam M R, Ali M M, Lai M H, et al. *Senso*, 2014, 14: 7451
4. Costa G K, Gouvêa P M, Soares L M, et al. *OExpr*, 2016, 24: 14690
5. Lawall J R. *JOSAA*, 2005, 22: 2786
6. Wildi F, Pepe F, Chazelas B, et al. *Proceedings of Conference on Ground-based and Airborne Instrumentation for Astronomy III*. San Diego, California, United States: SPIE, 2010, 7735: 1853
7. Bauer F F, Zechmeister M, Reiners A. *A&AC*, 2015, 581: A117
8. Cersullo F, Coffinet A, Chazelas B, et al. *A&AC*, 2019, 624: A122
9. 刘桐君, 叶慧琪, 唐靓, 等. 光子学报, 2023, 52: 0552203
10. Terrien R C, Ninan J P, Diddams S A, et al. *AJ*, 2021, 161: 252
11. Yüksel K, Wuilpart M, Mégret P. *OExpr*, 2009, 17: 12161
12. Deng Z, Liu Z, Gu S, et al. *OptCo*, 2020, 455: 124556
13. Stürmer J, Seifahrt A, Schwab C, et al. *JATIS*, 2017, 3: 048001
14. Zhao S, Suo L, Xu H, et al. *OptCo*, 2022, 508: 127737
15. Fredrick C, Olsen F, Terrien R, et al. *Optic*, 2022, 9: 1037
16. Foi A, Trimeche M, Katkovnik V, et al. *ITIP*, 2008, 17: 893
17. Ding M, Komanec M, Suslov D, et al. *JLwT*, 2020, 38: 4649
18. Michaud-Belleau V, Numkam Fokoua E R, Horak P, et al. *PhRvA*, 2022, 106: 023501

19. Wakaki M, Shibuya T, Kudo K. *Physical Properties and Data of Optical Materials*. Boca Raton: CRC Press, 2018: 399
20. Leviton D B, Frey B J. *Proceedings of Conference on Optomechanical Technologies for Astronomy*. Orlando, Florida, United States: SPIE, 2006, 6273: 800
21. Ciddor P E. *ApOpt*, 1996, 35: 1566